Performance Analysis and Test Research of PEMFC Oil-Free Positive Displacement Compressor for Vehicle

Jian Sun , **Bin Peng** * and **Bingguo Zhu**

School of Mechanical and Electrical Engineering, Lanzhou University of Technology, Lanzhou 730050, China; lutpb_sj_2016@163.com (J.S.); 13919835339@163.com (B.Z.)
* Correspondence: pengb2000@lut.edu.cn; Tel.: +86-93-1517-2154

Abstract: In order to study the matching characteristics of the positive displacement air compressor and the PEMFC (proton exchange membrane fuel cells), air supply subsystem, the basic operating performance parameters of the scroll and single-screw air compressors were analyzed with the focus on the oil-free double-wrap scroll compressor. According to the thermodynamic model and three-dimensional unsteady-state numerical simulation, the variation of the temperature, pressure, and velocity was obtained. Besides, under the rated operating condition of the compressor, the inlet and outlet mass flow rate of the fluid in the working chamber with the orbiting angle of the crank was achieved. Based on the built test platform, the actual working process of scroll and screw compressors was analyzed. This study indicates that the volume flow can be significantly increased by improving the speed of the positive displacement compressor. Based on the experimental measurement, when the height of the scroll tooth of the scroll compressor increases by 5 mm, the volume flow of the prototype SC2 increases by 0.17 m^3/min and the exhaust temperature is reduced by 13 °C at the rated speed.

Keywords: PEMFC; positive displacement compressor; scroll compressor; screw compressor; computational fluid dynamics; test research

1. Introduction

The HFC (hydrogen fuel cell) system is a device that converts part of the difference of the chemical energy of the water vapor molecule and the hydrogen molecule and oxygen half molecule into electrical work [1]. Its end product is water which does not affect the environment, and oxygen (one of its raw materials) can be obtained from the air [2]. Thus, this system can reduce the cost of the entire fuel cell system. The main component of the HFC system is the air supply subsystem. The airflow and intake pressure largely determine the power generation efficiency and power generation capacity of the entire system. Since the discharge pressure of the positive displacement air compressor is handy to control, the compressor can meet the needs of higher intake pressure of the HFC air supply subsystem for vehicles. As typical positive displacement compressors, scroll and screw compressors are more suitable for HFC power generation systems of vehicles with a stacking power of less than 100 kW. With the maturity of oil-free compressor technology, oil-free compressors can be applied in hydrogen fuel cell power generation systems that require extremely high air quality [3,4].

With few working parts, a simple structure, and favorable force balance during working, the CP-type single-screw compressor can be applied to the vehicle PEMFC system [5,6]. The fuel cell system requires intake pressure (below 0.3 MPa), volume flow (greater than 4 m^3/min), together with a specific size and structure of the air compressor. The single-scroll compressor cannot meet the basic needs of the system, while the double-wrap scroll compressor has a low pressure ratio and large displacement, so the double-wrap scroll compressor covers a wide range of application prospects in fuel cell systems. While

the basic geometric parameters remain unchanged, the volume flow of the scroll compressor can be increased by increasing the tooth height and rotational speed of the scroll compressor. Since the operating principles of double-wrap and single-scroll compressors are basically the same, the research theory of single-scroll compressors can be used for research and analysis [7–9].

Peng et al. [10] quantitatively analyzed the influence of basic geometric parameters on the performance of double-wrap scroll compressors. Cardone et al. [11] established a semi-empirical thermodynamic model of scroll compressors and evaluated the accuracy of the model with experimental data.

The working chamber of the compressor is closed, so it cannot be studied by direct measurement. Therefore, the fluid working medium in its working chamber can be analyzed by CFD methods [12,13]. Ooi et al. [14] used the CFD method to analyze the two-dimensional non-steady-state numerical simulation of the scroll compressor, and found that the heat transfer and leakage between the working chambers have an impact on the fluid distribution in the working chamber, and that the pressure of the distribution has the least impact in the chamber. Wang et al. [15,16] found that the scroll compressor fluid domain consisting of structured grids allows for more accurate calculations. Due to the appearance of the vortex, there is a pressure loss in the discharge process. Based on numerical simulation, Sun et al. [17] found that the mass exchange between the adjacent working chambers of the scroll compressor has little influence on the pressure distribution in the working chamber but a greater effect on temperature and velocity. Zhao et al. [18] conducted three-dimensional unsteady-state numerical simulation of compression and found that the shape and area of the compressor inlet will affect the pressure distribution in the discharge chamber. Fadiga et al. [19] proposed a special grid generation method based on the open source CFD software OpenFOAM, which can quickly generate a fluid domain grid that matches the working fluid, so that the grid can make the scroll machinery's working area match well with the fluid working medium. Cavazzini et al. [20] combined CFD and PSO (particle swarm optimization) algorithms and found that the radius of gyration, the number of scroll teeth, and the size of the exhaust port all have an impact on the output characteristics of the scroll compressor. Rak et al. [21] found that the Nusselt numbers calculated using CFD deviate from the values obtained by the formula due to the consideration of the influence of heat transfer and leakage on the scroll compressor in the calculation process. Giovanna et al. [22] found that the selection of the calculation model has an impact on the distribution of the flow field in the compressor chamber, and it also affects the mass flow of the scroll compressor inlet and outlet mass flow; moreover, the *k*-model is more suitable for scroll machinery. Zheng et al. [23,24] studied the flow field distribution of the CO_2 refrigeration scroll compressor during the working process; internal leakage, under-compression, and over-compression all have an impact on the flow field in the chamber during the working process; in addition, this will make the local temperature too high in the chamber. Wang et al. [25] designed a new type of asymmetric double-wrap scroll compressor via the midline method, which has improved the compressor's displacement and internal volume ratio.

At present, there are few instances of literature that can comprehensively study the performance characteristics of double-wrap scroll compressors from the aspects of thermodynamic model, numerical simulation, and experimental research. In this paper, a three-dimensional unsteady-state numerical simulation of a PEMFC air supply subsystem (suitable for a 45 kW stack) of oil-free double-wrap scroll compressor with a volume flow $\dot{q}_v = 4 \text{ m}^3/\text{min}$ was studied, under rated operating function. Through experiments, basic output performance parameters of scroll compressors were studied, and the basic performance parameters of oil-free double-wrap scroll compressors and CP-type single-screw compressors were compared with the variation of volume flow. In the previous research and literature, there were few simultaneous quantitative analyses and comparisons on the basic performance of oil-free double-wrap scroll and screw compressors. However,

this paper can provide a certain theoretical basis for the selection and optimization of PEMFC oil-free scroll and screw compressors.

In this paper, the performance analysis and test research of PEMFC oil-free positive displacement compressor for vehicle are performed. The paper is organized as follows: First, the basic geometric parameters of the scroll and screw compressor are defined. Based on calculus, we derived the expression of working chamber volume for the oil-free double-wrap scroll compressor. Second, the thermodynamic model of an oil-free double-wrap scroll compressor was established under ideal working conditions. Third, the three-dimensional unsteady-state numerical simulation was performed to analyze the internal flow characteristics of the compressor, which include the distribution of flow field, temperature field, and pressure field. Finally, we built a performance test platform for the prototype; the volume flow, discharge temperature, and vibration value were obtained, and we made a comparison between the scroll compressor and single-screw compressor. We also provided a geometry model of the double-wrap scroll and CP-type single-screw compressor.

The prototype of the scroll profile used in the test was composed of a circular involute. Its basic geometric parameters are depicted in Table 1; the scroll profile of the double-wrap scroll compressor is shown in Figure 1a. The basic geometric parameters of the CP-type single-screw compressor are shown in Table 2; Figure 1b illustrates the basic structure of the screw and star-wheel of the screw compressor.

Table 1. Basic parameters of scroll tooth geometry.

Paraments	Symbol	Value	Units
Base circle radius	r_b	9.231	mm
Involute angle	α	0.244	rad
Revolution radius	r_{or}	10.000	mm
Starting angle of involute	φ_s	0.785	rad
End angle of involute	φ_e	3.336	rad

Table 2. Basic geometric parameters of the single-screw compressor.

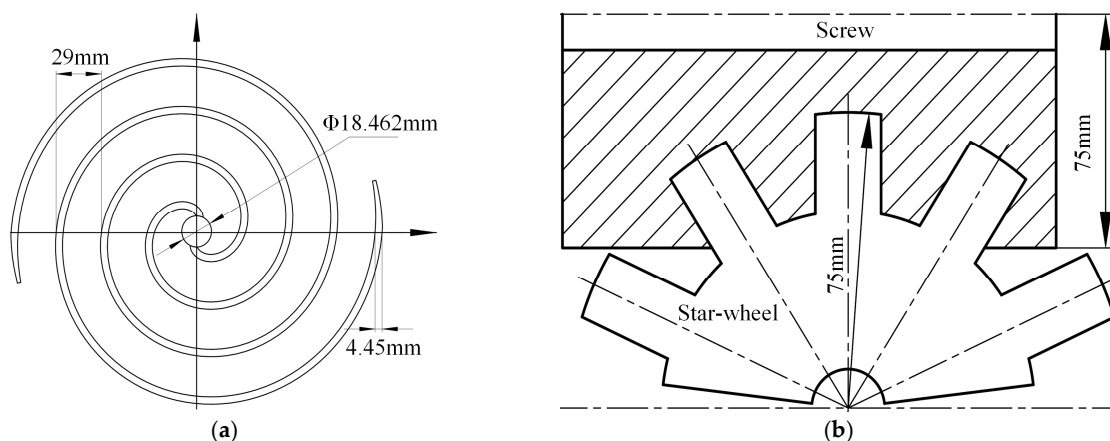| Paraments	Symbol	Value	Units
Screw tooth groove number	z_1	6	-
Number of star gears	z_2	11	-
Screw tip circle diameter	d_1	150	(mm)
Diameter of tip circle of star gear	d_2	150	(mm)
Screw length	L	153	(mm)

Figure 1. Compressor geometry: (**a**) scroll tooth profile; (**b**) CP-type single-screw compressor.

2. Double-Wrap Scroll Compressor

2.1. Working Chamber Volume

Since the research and test prototype is applied to the vehicle PEMFC system, it is necessary to analyze and study the changes in the working chamber volume of the compressor according to the requirements of the fuel cell stack for the volume flow and exhaust pressure of the air supply subsystem; the calculation equations for the working chamber volume of the oil-free double-wrap scroll compressor are as follows [10]:

Discharge chamber:

$$V_d = hp_t(p_t - 2t)(4\varphi_s + 5\pi) \tag{1}$$

Compression chamber:

$$V_i = hp_t(p_t - 2t)\left[\varphi_e - \theta - \frac{5 + 2(i-1)}{4}\pi\right] \tag{2}$$

Suction chamber:

$$V_s = \tfrac{1}{8}r_b\theta(4\phi_e - 2\theta - \pi)(p_t - 2t) \\ + \tfrac{1}{2}r_b(\tfrac{1}{2}\pi - 2r_b\alpha) \cdot [2(1 - \cos\theta) - 2(\varphi_e - \pi)\sin\theta - \tfrac{1}{4}\pi\sin 2\theta] \tag{3}$$

where, i—is the i-th working chamber of the compressor; θ—is orbiting angle, $°$; p_t—is the scroll pitch, mm.

2.2. Thermodynamic Model

In the thermodynamic model of the scroll compressor, initial conditions are set as: the initial inlet pressure p_s = 0.1 MPa, the initial inlet temperature T_s = 300 K, the working medium is air, which is assumed to be an ideal gas. The scroll compressor is variable in actual operation, and its pressure and temperature are as follows:

Pressure:

$$p_i = p_s(V_d/V_i)^k \tag{4}$$

Temperature:

$$T_i = T_s(V_d/V_i)^{((\kappa-1)/\kappa)} \tag{5}$$

where, κ—is variability index.

2.3. Volume Flow

The displacement of the scroll compressor is an important indicator of its performance. In the actual operation of the scroll compressor, the actual displacement is less than the theoretical displacement due to irreversible losses such as leakage. The calculation equations are as follows:

Theoretical volume flow:

$$q_{v,\text{th}} = nV_s \tag{6}$$

Actual volume flow:

$$q_v = \eta_v q_{v,\text{th}} \tag{7}$$

where, η_v—is volumetric efficiency; n—rotational speed, r/min.

2.4. Optimization and Improvement

After prototype 1 was designed and tested, problems occurred in the designed oil-free double-wrap scroll compressor, such as low volume flow, high discharge temperature, and high driving motor temperature; in particular, the prototype was difficult to match with the PEMFC air supply subsystem. Therefore, prototype 2 was designed after optimization to solve these problems. The heights of the scroll teeth of prototype 1 and prototype 2 are 60 mm and 65 mm, respectively. In addition, prototype 2 was added with a liquid cooling system to reduce the temperature of the driving motor. SC1 and SC2 are referred to as prototype 1 and prototype 2, respectively. The two prototypes are shown in Figure 2.
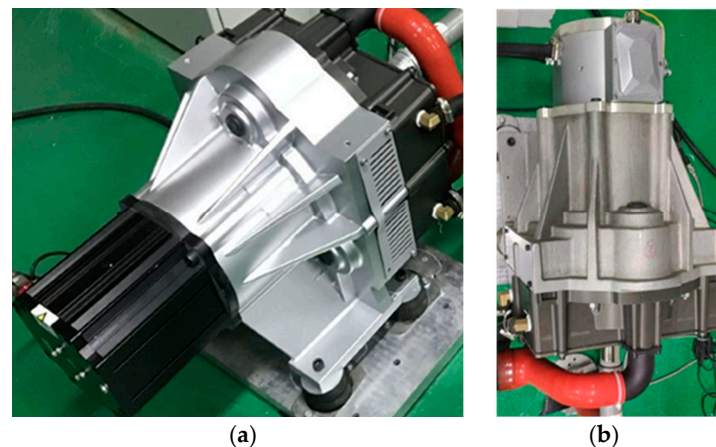
Figure 2. Test prototypes: (**a**) prototype 1-SC1; (**b**) prototype 2-SC2.

2.5. Discussion and Analysis

2.5.1. Volume of the Working Chamber

Figure 3 shows the variation of the working chamber volume of the double-wrap scroll compressor with the orbiting angle of the crankshaft. *V* and ΔV are the difference between the volume and volume of the working chamber, respectively. As shown in Figure 3, in the suction process, the working chamber volume changes with the increase of orbiting angle. When the crankshaft turns to the suction end angle θ_s, the suction process ends and the compression process begins. At different tooth heights, the maximum suction volume difference of the suction chamber is 0.06315 dm^3. During compression and discharge, with the change of the orbiting angle, the volume of the scroll compressor working chamber continues to decrease until the fluid working medium is completely discharged from the chamber; at this time, one cycle of the compressor's working process ends. The discharge process begins when the spindle rotates to the discharge starting angle θ_d.
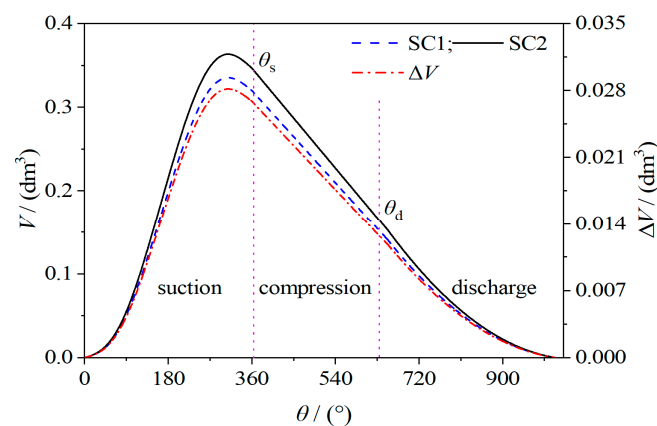

Figure 3. Working chamber volume.

2.5.2. Temperature and Pressure

Figure 4 shows the variation of the working fluid temperature *T* and pressure *p* in the working chamber of the scroll compressor with the orbiting angle of the crankshaft. It can be seen from Equations (4) and (5) that the pressure and temperature of the fluid working medium in the working chamber of the scroll compressor during the ideal compression work process have nothing to do with the height of the scroll teeth, but are only related to the basic geometric design parameters of the compressor, which is only related to the basic geometric parameters. In the theoretical operation process of the scroll compressor, the changing trend of temperature and pressure was basically the same. During the suction and discharge process, the temperature and pressure remained unchanged because the suction

and discharge chambers were connected to the external environment. In the compression process, the temperature and pressure in the compression chamber were affected by the volume of the working chamber. Since the volume of the scroll compressor working chamber continued to decrease with the orbiting angle of the crankshaft, the temperature and pressure continued to rise.
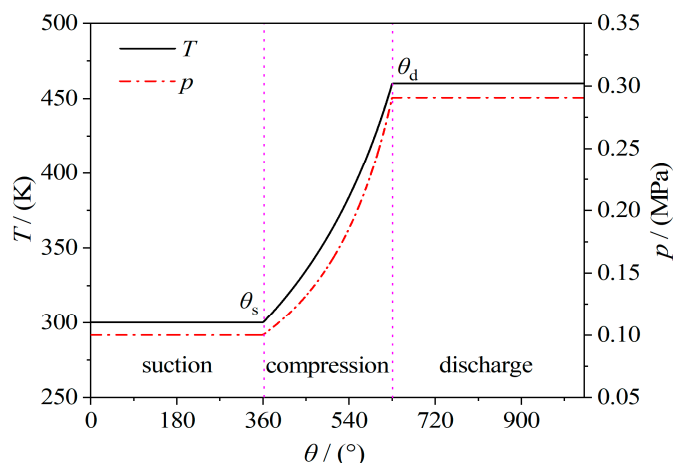

Figure 4. Temperature and pressure of ideal working process.

2.5.3. Theoretical Volume Flow and Volumetric Efficiency

Figure 5 shows the variation of the theoretical volume flow $q_{v,\text{th}}$ and volumetric efficiency η_v of the scroll compressor with the rotational speed, respectively. $\Delta q_{v,\text{th}}$ and $\Delta \eta_v$ are the difference between the theoretical volume flow and volumetric efficiency of SC1 and SC2, respectively. As shown in Figure 5a), at the same speed but different tooth heights, the larger the theoretical volume flow of the compressor, the greater the volumetric efficiency. At a constant tooth height, as the speed gradually increases, the theoretical volume flow also increases. According to Figure 5b, at the same tooth height, higher speed means higher volumetric efficiency because internal leakage is too late to occur at high speeds. When the rotational speed increases to 1200 r/min, the scroll compressor volumetric efficiency tends to stabilize and no longer increases significantly. The volumetric efficiency of the compressor is mainly affected by the direction of the actually measured volumetric flow. The compressor's speed, sealing structure, and accuracy of the flowmeter all affect the measured volumetric flow. The volume flow of prototype SC2 is 0.36 m³/min, higher than that of SC1, and the maximum efficiency of prototype SC2 only increased by 0.02.
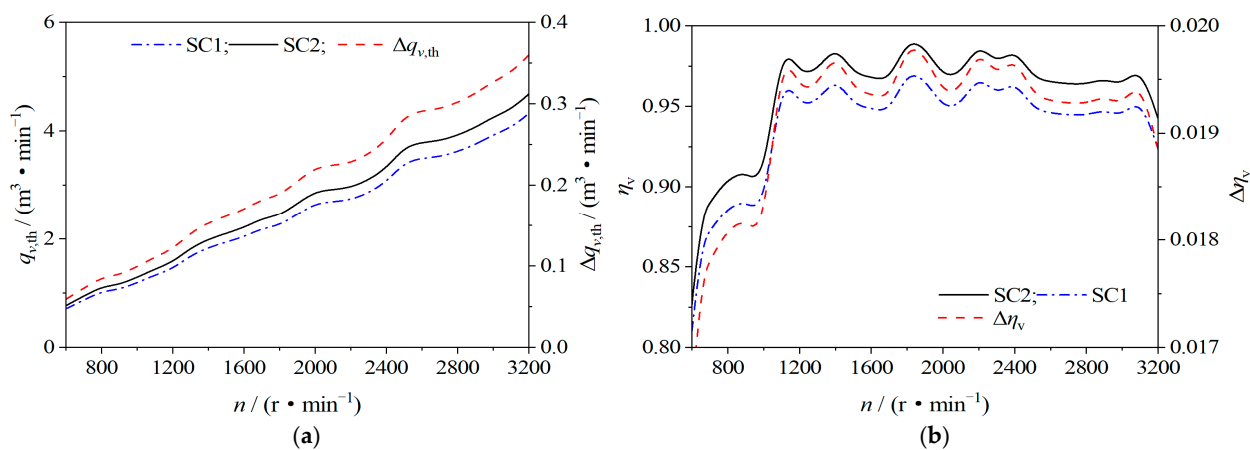

Figure 5. Theoretical volume flow and volumetric efficiency: (**a**) theoretical volume flow; (**b**) volumetric efficiency.

3. Numerical Simulation of Double-Wrap Scroll Compressor

3.1. Governing Equation

In the numerical simulation of the scroll compressor, the interaction between temperature, pressure, and velocity and the fundamental laws of physics such as the mass, momentum, and energy conservation equations should be considered. The basic equations are as follows [26]:

Mass equation:

$$-\frac{\partial \rho}{\partial \bar{t}} + \frac{\partial(\rho \bar{u})}{\partial x} + \frac{\partial(\rho \bar{v})}{\partial y} + \frac{\partial(\rho \bar{w})}{\partial z} = 0 \tag{8}$$

Energy equation:

$$\frac{\partial(\rho \bar{T})}{\partial \bar{t}} + \frac{\partial(\rho \bar{u}\bar{T})}{\partial x} + \frac{\partial(\rho \bar{v}\bar{T})}{\partial y} + \frac{\partial(\rho \bar{w}\bar{T})}{\partial z} = \frac{\partial}{\partial x}\left(\frac{k}{c_p}\frac{\partial \bar{T}}{\partial x}\right) + \frac{\partial}{\partial y}\left(\frac{k}{c_p}\frac{\partial \bar{T}}{\partial y}\right) + \frac{\partial}{\partial z}\left(\frac{k}{c_p}\frac{\partial \bar{T}}{\partial z}\right) + S_r \tag{9}$$

Momentum equation:

$$\begin{cases} \frac{\partial(\rho \bar{u})}{\partial \bar{t}} + \operatorname{div}(\rho \overline{uu}) = -\frac{\partial \bar{p}}{\partial x} + \frac{\partial \tau_{xx}}{\partial x} + \frac{\partial \tau_{xy}}{\partial y} + \frac{\partial \tau_{zx}}{\partial z} + F_x \\ \frac{\partial(\rho \bar{v})}{\partial \bar{t}} + \operatorname{div}(\rho \overline{vu}) = -\frac{\partial \bar{p}}{\partial y} + \frac{\partial \tau_{xy}}{\partial x} + \frac{\partial \tau_{yy}}{\partial y} + \frac{\partial \tau_{zy}}{\partial z} + F_y \\ \frac{\partial(\rho \bar{w})}{\partial \bar{t}} + \operatorname{div}(\rho \overline{wu}) = -\frac{\partial \bar{p}}{\partial z} + \frac{\partial \tau_{xz}}{\partial x} + \frac{\partial \tau_{yz}}{\partial y} + \frac{\partial \tau_{zz}}{\partial z} + F_z \end{cases} \tag{10}$$

where, $\bar{u}$, $\bar{v}$ and $\bar{w}$—are the components of the velocity vector u in the x, y, and z directions respectively; ρ—is the density, $\bar{t}$—is the time, $\bar{p}$—is the pressure; τ_{xx}, τ_{xy} and τ_{zx}—are the components of the viscous stress; F_x, F_y and F_z—are the physical force on the micro-element body; c_p—is the specific heat capacity; $\bar{T}$—is the temperature; k—is the heat transfer coefficient; S_r—is the viscous dissipation term.

3.2. Grid Division and Independence Verification

3.2.1. Fluid Domain Grid Division

For the convenience of grid division, the entire fluid domain was divided into three areas: inlet pipe, working chamber, and outlet pipe [27]. The particularity of the scroll compressor fluid domain contributed to the working chamber grid. The grid used mesh stretching in ICEM to generate volume grids. The inlet pipe and outlet pipe were composed of unstructured hexahedral grids, and the fluid domain grid was composed of unstructured triangular prism grids. The fluid domain is shown in Figure 6.
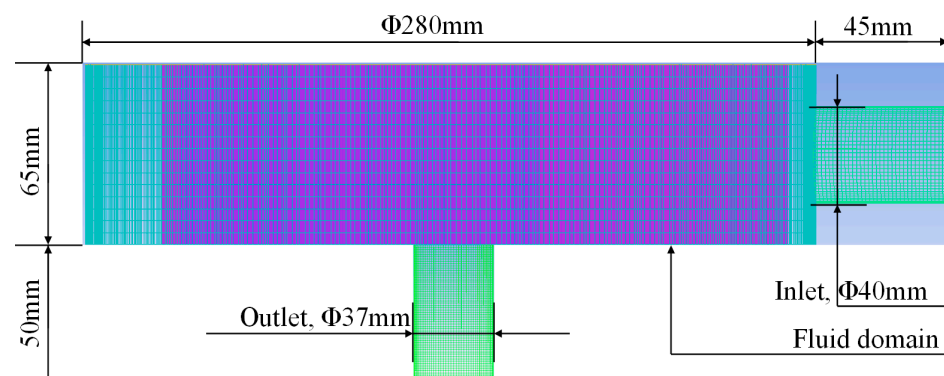

Figure 6. Fluid domain volume grid.

3.2.2. Grid Independence Verification

Figure 7 shows the changing trend of the outlet mass flow of the oil-free double-wrap scroll compressor SC2 with the number of fluid domain grids. After dividing the grid into the computational fluid domain, the final selection of the grid is based on a combination

of calculation time and computing resources. The grid number of the model is 5,716,526 when the number of grid-stretching layers is 15. Similarly, it can be obtained that the grid number of SC1 is 5,045,765 when the number of grid-stretching layers is 15. Table 3 shows the number of grids in each domain of compressor SC2.
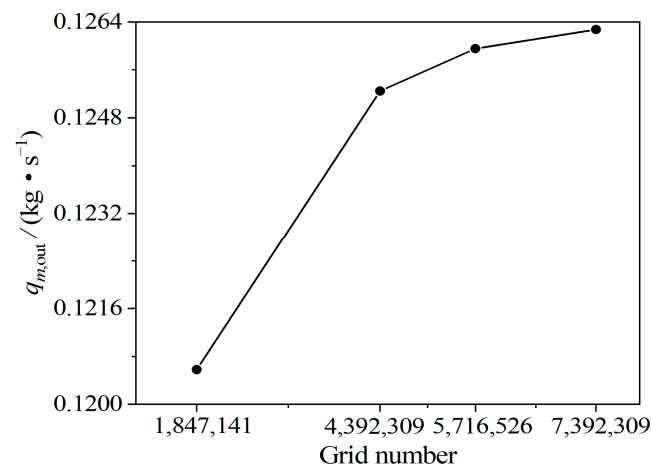

Figure 7. Grid independence verification.

Table 3. Number of grids in each fluid domain.

Number	Total Elements	Total Nodes
Inlet pipe	23,337	10,189
Working chamber	5,613,089	2,608,404
Outlet pipe	80,100	13,762
Total	5,716,526	2,635,355

3.3. Calculation Method and Boundary Conditions

In the three-dimensional unsteady-state numerical simulation of the scroll compressor, the turbulent flow model used the $\kappa - \varepsilon$ RNG model, the near-wall surface used the standard wall function, the fluid heat transfer used the high-order second-order upwind model, and the discrete term used the central difference format and the PISO! algorithm for unsteady-state numerical simulation. The UDF in FLUENT controlled the movement of the orbiting scroll. The pressure was the boundary condition of the inlet and outlet, and the rotational speed was set to 3000 r/min.

3.4. Discussion and Analysis

3.4.1. Distribution Contour of Fluid in the Working Chamber

Figure 8 shows the temperature, pressure, and velocity variation in the working chamber of the double-wrap scroll compressors SC1 and SC2 when the orbiting angle is 360°. At the same tooth height, the proximity to the central chamber indicates higher temperature, pressure, and velocity in the chamber. Due to leakage between adjacent working chambers, there exists mass exchange between the working chambers, making the temperature and velocity distribute inconsistently, and internal leakage has little effect on the pressure in the working chamber. Because four discharge chambers of the double-wrap scroll compressor were not connected to the outlet simultaneously during operation, the movement characteristics of the fluid working medium in the exhaust chamber were inconsistent. At different tooth heights, there are differences in the distribution of temperature, pressure, and velocity in the discharge chamber. The closer the scroll tooth wall, the greater the change in temperature and velocity. In the working chamber, the temperature of prototype SC2 increased by 28.42 K, the pressure increased by 1.5 kPa, and the velocity increased by 19.34 m/s, compared with SC1.
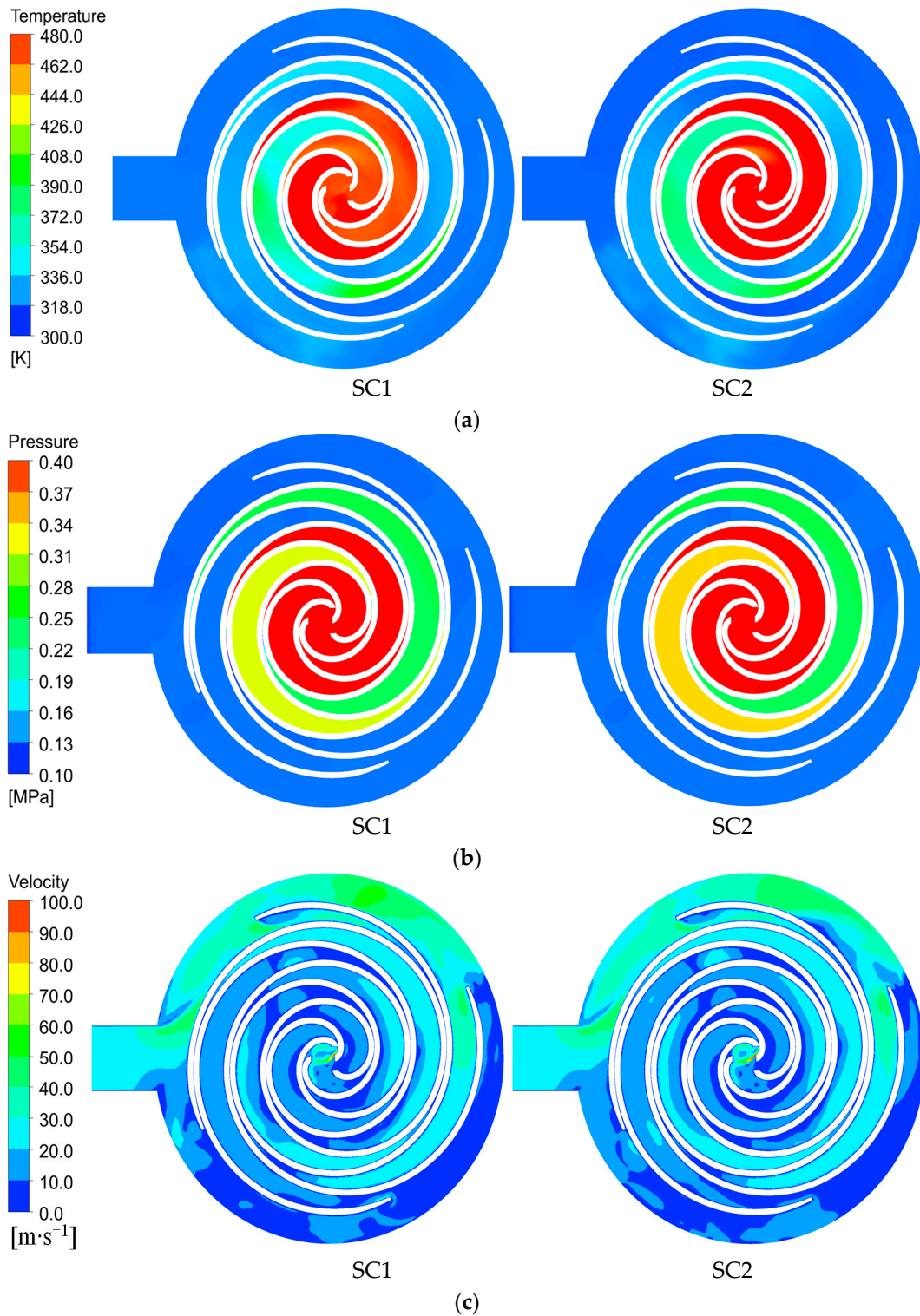
Figure 8. Temperature, pressure, and velocity contour in the working chamber: (**a**) temperature contour; (**b**) pressure contour; (**c**) velocity contour.

3.4.2. Inlet and Outlet Mass Flow

Figure 9a,b show the variation of the inlet and outlet mass flow of the double-wrap scroll compressor with the orbiting angle of the crankshaft, $q_{m,\mathrm{in}}$ and $q_{m,\mathrm{out}}$ as the inlet and outlet mass flow. As show in the figure, the fluctuating trend of the flow rate at the

inlet is not significant; at the outlet, the orbiting scroll periodically shields the discharge port, and it will interfere with the exhaust process of the working fluid at the outlet, so the outlet mass flow fluctuates greatly. Due to the internal leakage between adjacent working chambers, the inlet mass flow is greater than the outlet mass flow. Figure 9c shows the variation of the SC2 inlet and outlet mass flow with the orbiting angle, Δq_m is the difference in the inlet and outlet mass flow of SC2. The average inlet mass flow is 0.139631 kg/s, the average outlet mass flow is 0.1389624 kg/s, and the flow difference is 6.686×10^{-6} kg/s. The radial leakage produced by the oil-free scroll compressor is unavoidable; the leakage between the adjacent working chambers of the scroll compressor leaks from the high-pressure chamber to the low-pressure chamber. During the cycle, part of the fluid in the working chamber will undergo repeated compression, so that the compressor mass flow of the outlet will be slightly decreased.
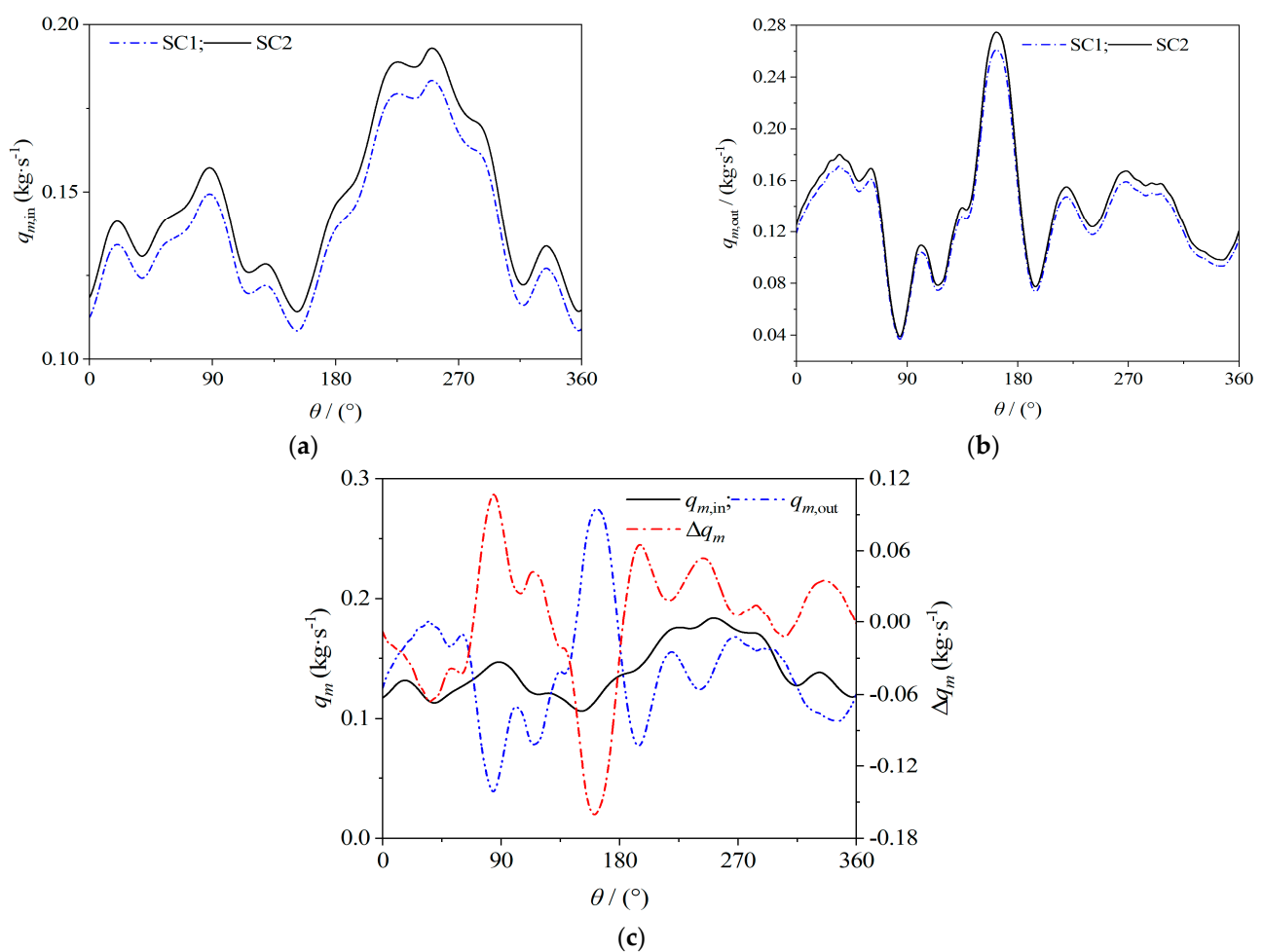

Figure 9. Inlet and outlet mass flow: (**a**) inlet mass flow; (**b**) outlet mass flow; (**c**) SC2 of inlet and outlet mass flow.

3.4.3. Inlet and Outlet Velocity

Figure 10a–c show the variation of the inlet and outlet velocity of the scroll compressor with the orbiting angle of the crankshaft and SC2 inlet and outlet velocity, respectively. v_{in} and v_{out} are the inlet and outlet velocity, Δv is the difference in the inlet and outlet velocity, respectively. According to Figure 10, after a cycle of the scroll compressor, the outlet velocity is greater than the inlet velocity due to the increase in pressure at the outlet and the decrease in the diameter of the discharge port. Due to the interference of the orbiting scroll on the discharge port, the outlet velocity is more volatile. The maximum difference between the inlet and outlet velocity of SC1 and SC2 is 1.125 m/s and 1.950 m/s,

respectively. The average velocities of SC2 inlet and outlet are 29.353 m/s and 36.587 m/s, respectively. Since the orbiting scroll will periodically affect the intake and exhaust process during its rotation, when the orbiting scroll has different disturbances to the intake process, the inlet flow rate will increase or decrease. The degree of shielding of the exhaust port by the scroll teeth has a great influence on the outlet velocity, which will make the change trend of the outlet velocity different.
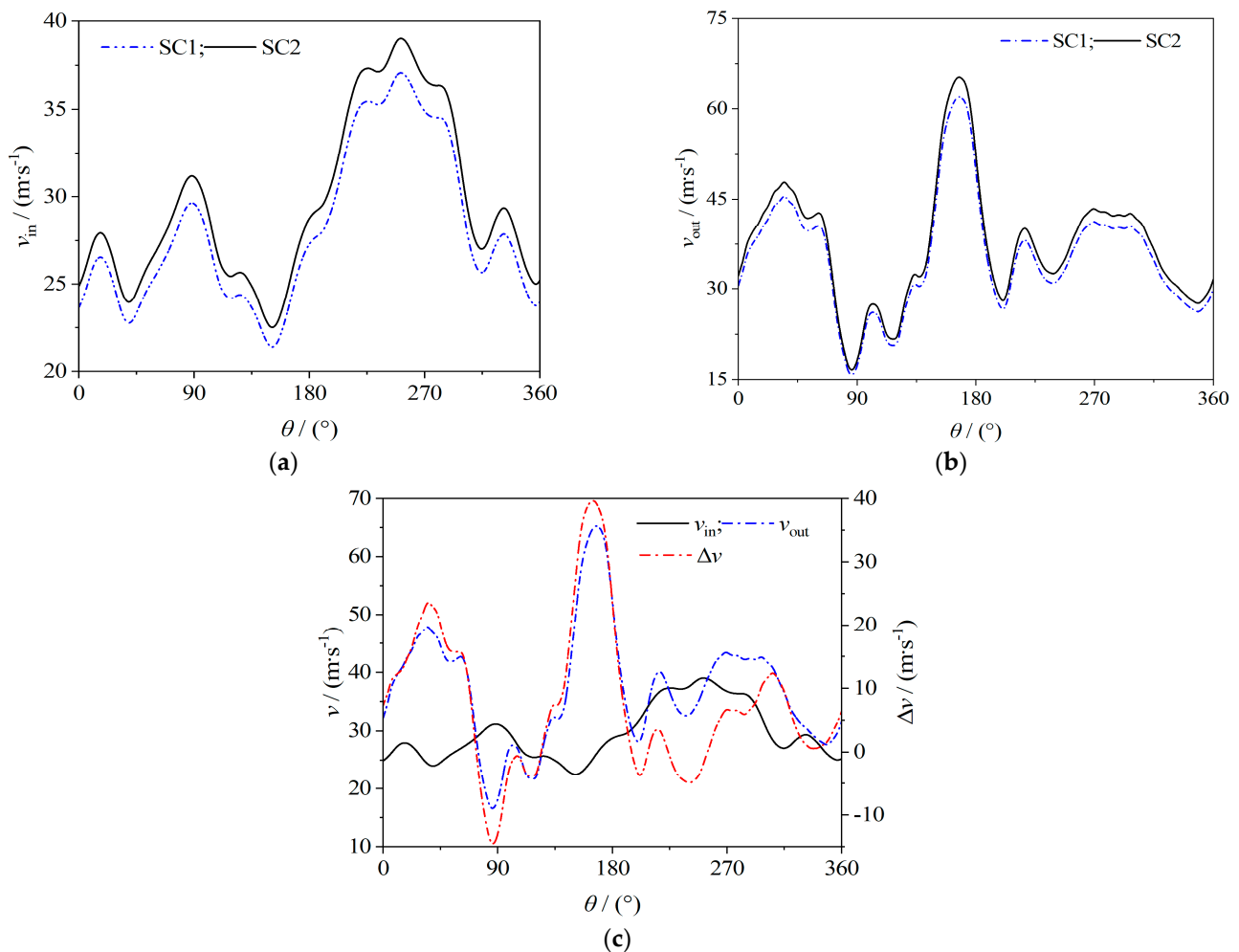

Figure 10. Inlet and outlet velocity: (**a**) inlet velocity; (**b**) outlet velocity; (**c**) SC2 of the inlet and outlet velocity.

4. Test Research

Figure 11 shows the test schematic of the oil-free air compressor and the double-wrap scroll compressor test platform. In the test, the driving motor speed was adjusted by the motor driver, and the collected discharge temperature was cooled. Data of temperature after cooling were obtained by the data acquisition system. The gas tank of the scroll compressor test system and the liquid tank of the cooling system were placed outdoors. The cooling liquid of the scroll compressor and the driving motor was delivered by the circulating pump. The CP-type single-screw compressor was referred to as SC3. To compare the difference in basic output performance between scroll and screw compressors, the speed and discharge temperatures of compressors SC2 and SC3 at the same volume flow were compared through experiments. The variation of the body noise and the test principle of the screw compressor SC3 are shown in Figure 11a. The inlet pressure of the prototype is 0.1 MPa, the ambient temperature is 22 °C, and the rated speeds of SC1 and SC2 are both 3000 r/min. The screw compressor adopts the rated volume flow $\dot{q}_v = 4$ m^3/min, and the rated speed is 9500 r/min.
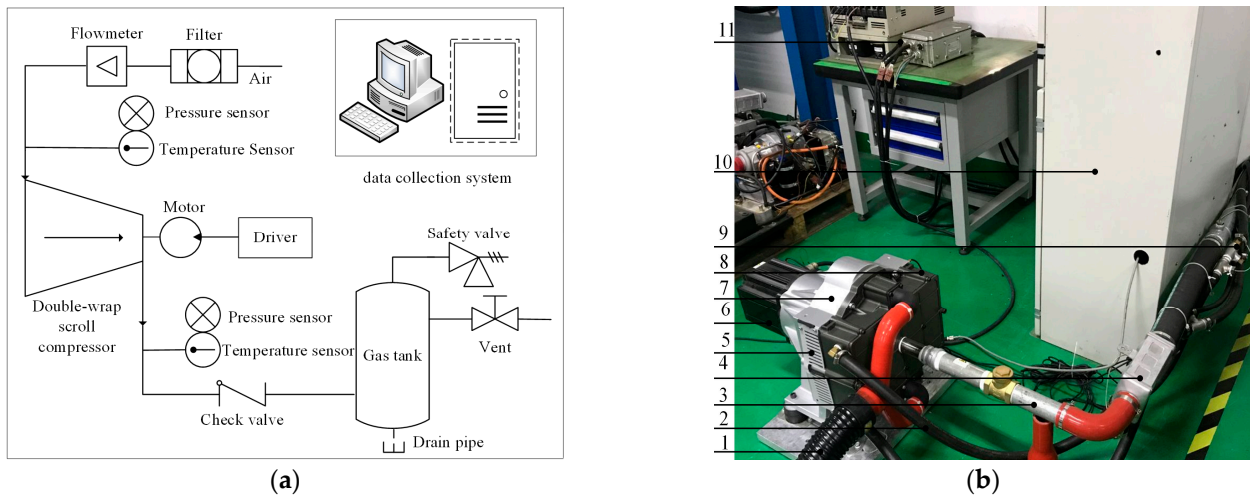
Figure 11. Test research: (**a**) test schematic; (**b**) double-wrap scroll compressor. 1—inlet pipe; 2—cooling pipe; 3—outlet pipe; 4—temperature sensor; 5—compressor; 6—motor; 7—vibration measuring point of the body; 8—vibration measuring point of the fixed scroll; 9—coolant temperature sensor; 10—data collection system; 11—motor driver.

4.1. Double-Wrap Scroll Compressor

4.1.1. Volume Flow

Figure 12 shows the variation of the inspiratory volume flow of prototypes at different rotational speeds; Δq_v is the difference in volume flow between SC1 and SC2. Actual volume flow is the focus of scroll compressor research, the volumetric flow measured in the experiment is the compressor inlet volume flow, and the flow meter is a vane air flow meter. The volume flow increases approximately linearly with the increase of speed. The volume flow rates of SC1 and SC2 increase with the improvement of scroll compressor speed accordingly. At the same speed, the maximum difference between SC1 and SC2 volume flow is 0.26 m^3/min; the minimum difference is 0.01 m^3/min; the maximum difference appears at a high rate of 2300 r/min; the minimum difference appears at a low rate of 1000 r/min. At the same tooth height, increasing the speed of the driving motor can increase the volume flow of the scroll compressor. At the same rotational speed, increasing the tooth height of the compression can also increase the volume flow.
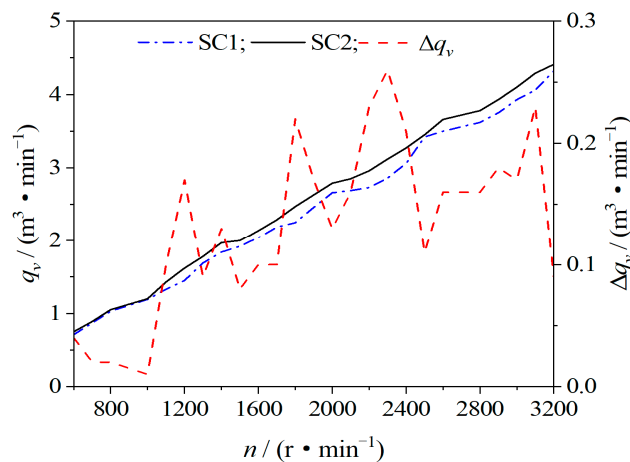

Figure 12. Volume flow.

4.1.2. Discharge Temperature

Figure 13 shows the variation of the discharge temperature of prototypes at different rotational speeds. T_{out} and ΔT_{out} are the discharge temperature of SC1 and SC2 and the

difference between the discharge temperature of SC1 and SC2. To operate the double-wrap scroll compressor safely and stably, the SC2 driving motor and SC1 and SC2 fixed scroll cooling measures adopted liquid circulation cooling, and the discharge temperature was collected after forced cooling. With the increase of the rotational speed, the discharge temperature of the prototype also increases. The maximum discharge temperature of SC1 is 54 °C, while the maximum discharge temperature of SC2 is 42 °C. Because the driving motor of SC2 also adopts cooling measures, the temperature of SC2 is reduced. When the rate is lower than 1800 r/min, the discharge temperature change trend of the two prototypes is basically the same because the liquid can dissipate in time. When the rate is higher than 1800 r/min, the discharge temperature of the two prototypes begins to increase due to the accumulation of liquid heat. SC1 discharge temperature begins to increase sharply, while the variation trend of SC2 discharge temperature is relatively gentle. At the maximum speed of 3200 r/min, the discharge temperature of SC1 and SC2 increases by 12 °C and 20 °C compared with the minimum discharge temperature, respectively.
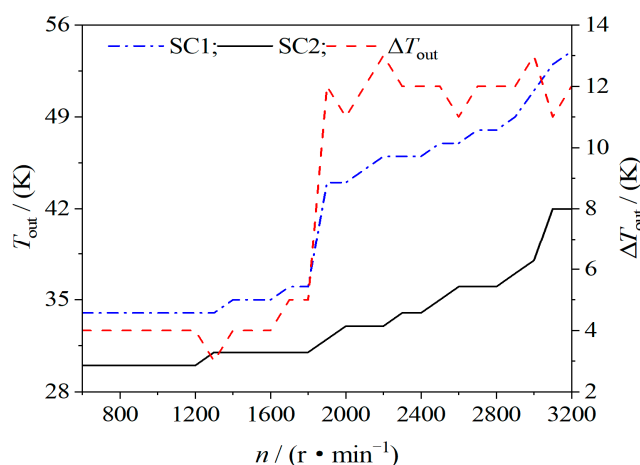

Figure 13. Discharge temperature.

4.1.3. Vibration Value

Figure 14 shows the vibration value of the body and fixed scroll of prototypes with the rotational speed. C_{body} and C_{fixed} are the vibration value of the scroll compressor body and the fixed scroll, respectively. The vibration measurement point of the body is located in the anti-rotation mechanism, which is the connection position of the fixed bracket of the compressor and the orbiting scroll assembly; the vibration value is affected by the motion of the body. The vibration measurement point of the fixed scroll is located at the cooling box, and the vibration value at this position is affected by the vibration of the body and the outlet pipe at the same time. The vibration value of the body and the fixed scroll increases with the increase of speed. After the tooth height increases by 5 mm, the maximum vibration value of the SC2 body and the fixed scroll becomes 4.3 mm and 7.4 mm, which is an increase of 0.1 mm and 0.3 mm compared with SC1, respectively. At the same speed, the vibration value of the SC2 body and the fixed scroll increases by 0.27 mm and 0.6 mm, respectively. At a certain speed, increasing the tooth height can increase the volume flow of the compressor, as well as the vibration value of the body and the fixed scroll. However, there is little impact on the operation of the whole machine.
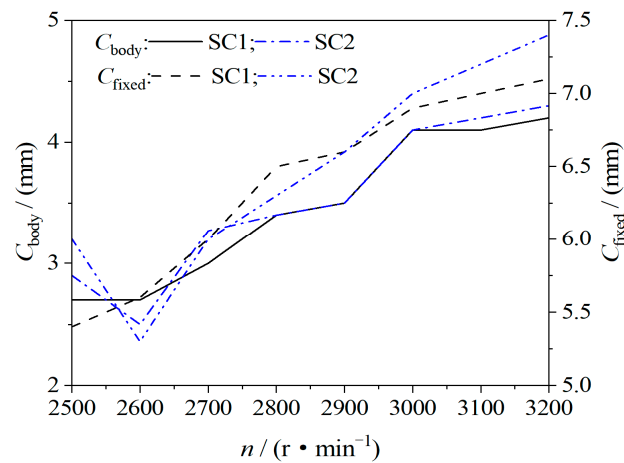
Figure 14. Vibration value of body and fixed scroll.

4.1.4. Driving Motor Power and Current

Figure 15a shows the variation of the driving motor power at a different speed. *P* and ΔP are the difference between the driving motor power and power of the prototypes SC1 and SC2, respectively. At the same speed, the driving motor power of SC2 is less than that of SC1, and the maximum difference in driving motor power is 2.5 kW. With the increase of the driving motor speed, the driving motor power also increases.
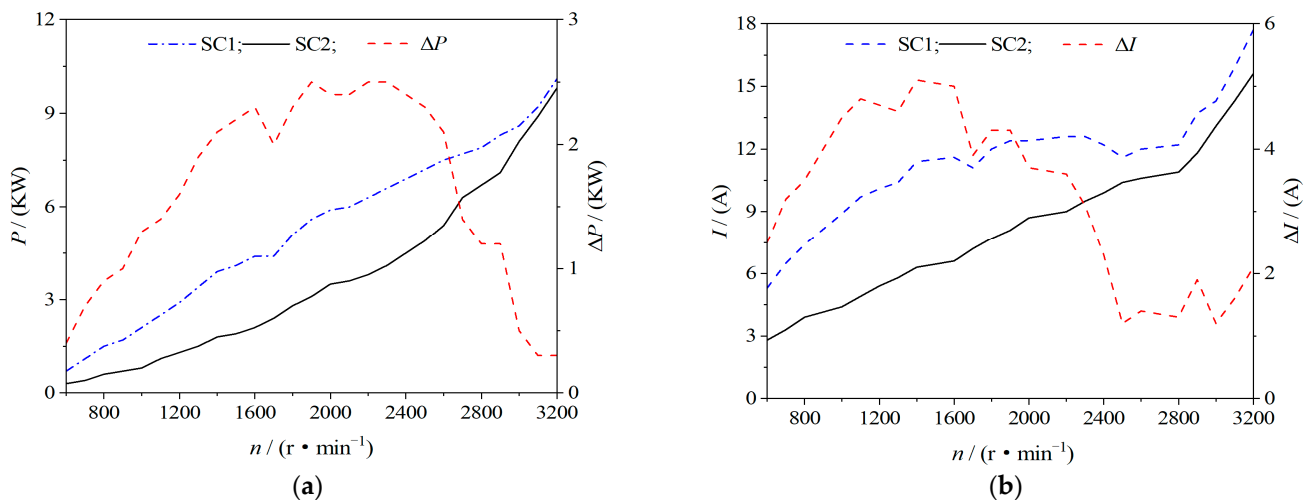

Figure 15. Driving motor power and current: (**a**) power; (**b**) current.

Figure 15b shows the variation of the driving motor current of prototypes at different speeds. *I* and ΔI are the difference between the driving motor currents and currents of prototypes SC1 and SC2, respectively. At the same speed, the SC2 driving motor current is less than the SC1 driving motor current, and the maximum difference in the driving motor current is 5.1 A. As the speed increases, not only the driving motor current but also the driving motor power increases. The temperature and current of the cooled driving motor are lower than the uncooled prototype.

4.2. Scroll and Screw Compressors

4.2.1. Volumetric Efficiency

Figure 16 shows the variation of volumetric efficiency of scroll and screw compressors with rotational speed. n_{SC2} and n_{SC3} are the speed of scroll and screw compressors, respectively. Scroll machinery is a variable displacement compressor; during the working process

of the compressor, the radial and axial clearances are reduced due to the temperature rise and deformation of the scroll tooth and the installation of sealing strips. The volume of the working chamber of the screw compressor does not change with the movement of the screw, so the meshing gap changes less during operation. According to Figure 16, the volumetric efficiency of scroll compressors has been higher than that of screw compressors. The average volumetric efficiency of screw compressors and screw compressors is 0.959 and 0.869, respectively. The volumetric efficiencies of scroll and screw compressors at the rated speeds are 0.963 and 0.937, respectively. When $n_{SC2} \geq 1200$ r/min and $n_{SC3} \geq 7500$ r/min, the volumetric efficiency of compressors tends to be stable without significant change.
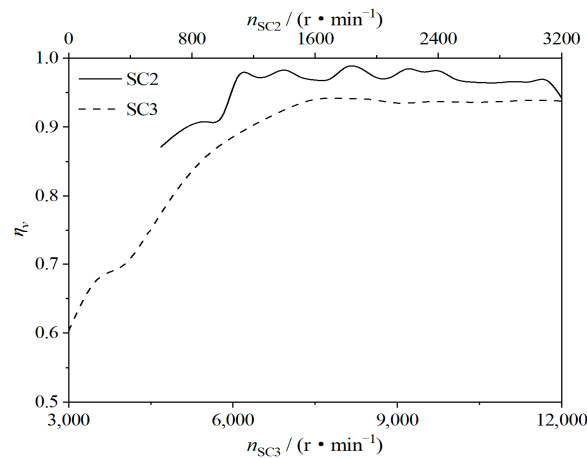

Figure 16. Compressor volumetric efficiency.

4.2.2. Rotational Speed and Noise

Figure 17a shows the variation of scroll and screw compressors' speed with volume flow. As shown in Figure 17, the volume flow is directly proportional to the compressor speed; namely, the larger the volume flow, the higher the compressor speed. At volume flow 4 m^3/min, the compressor speed increases due to irreversible losses such as internal leakage and suction pressure drop. The speed of the scroll and screw compressors is 3020 r/min and 9650 r/min, respectively.
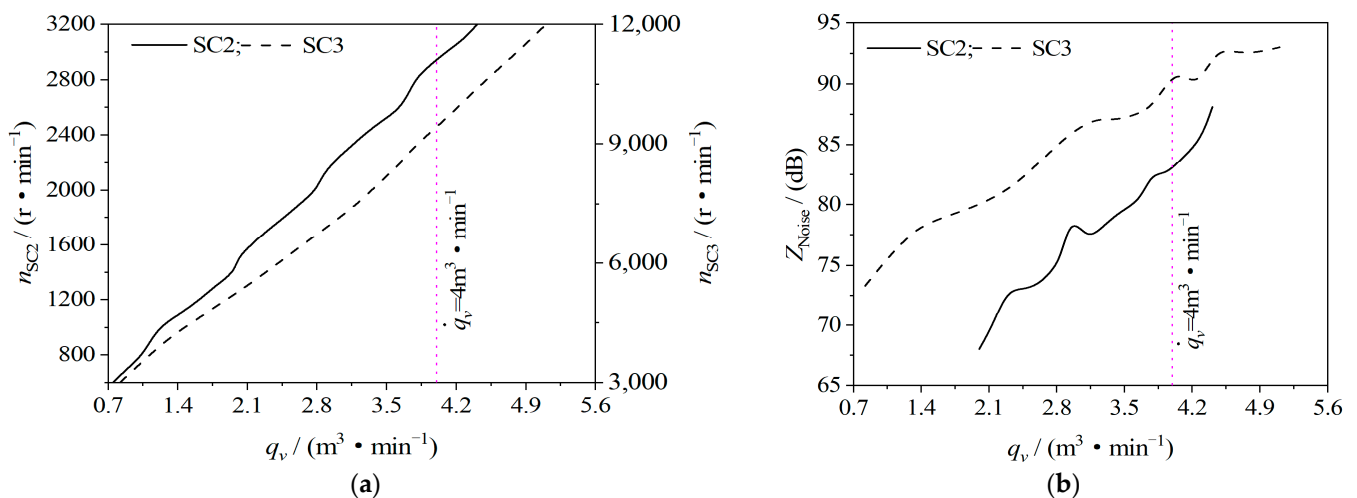

Figure 17. Compressor rotational speed and noise: (**a**) rotational speed; (**b**) noise.

Figure 17b shows the change of the noise generated by the scroll and screw compressors' bodies with volume flow. Since the volume flow of the compressor changes linearly

with speed, the larger the volume flow, the greater the noise generated by the body. When the volume flow is 4 m^3/min, the noises generated by the scroll and screw compressors are 82.5 dB and 91.4 dB, respectively. Therefore, excessive compressor noise should be further improved.

4.2.3. Discharge Temperature

Figure 18 shows the variation of the discharge temperature of the scroll and screw compressors with volume flow. $T_{SC2,out}$ and $T_{SC3,out}$ are the discharge temperature of the scroll and screw compressors, respectively. For positive displacement compressors, the volume flow is positively correlated with the compressor speed, and a high volume flow corresponds to a high rotational speed. The higher the speed, the greater the operating power of the compressor, the more power it generates, and the more heat the compressor generates from compressed gas, which increases the exhaust temperature. Since the scroll compressor cooling used liquid but the screw compressor cooling used air, the discharge temperature of the scroll compressor is much lower than that of the screw compressor. When the volume flow is 4 m^3/min, the discharge temperature of the scroll and screw compressors is 37 °C and 63.2 °C, respectively.
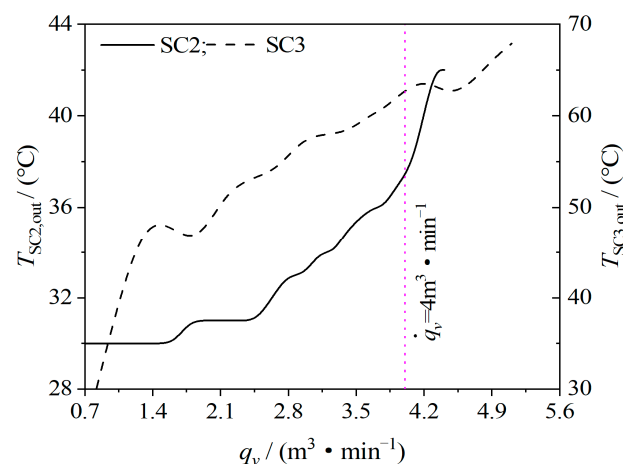

Figure 18. Compressor discharge temperature.

5. Conclusions

(1) The discharge pressure and volume flow are used as the objective function to measure the basic output performance parameters of the oil-free double-wrap scroll air compressor. The temperature, pressure, volume flow, and volume efficiency of the scroll compressor are all affected by the working chamber during the working process. The influence of volume is also affected by the basic geometric design parameters of the compressor.

(2) As the double-wrap scroll compressor has four exhaust chambers and the discharge port is large, the temperature, pressure, and velocity of each discharge chamber vary inconsistently. The inlet and outlet mass flows reach the maximum at crankshaft orbiting angle 250° and 160°, respectively. The discharge opening reaches the maximum when the spindle rotates to 120~186°. The mass exchange of working fluids between adjacent working chambers has a greater influence on the temperature and flow rate in the working chamber and less influence on the pressure.

(3) Based on the analysis and research of the built test platform, the maximum temperature of the SC2 discharge port was only 42 °C with liquid cooling measures for the scroll compressor and driving motor. After optimization, the scroll compressor is at a rated speed of 3000 r/min, the compressor discharge volume flow is 4.1 m^3/min, and the discharge temperature after cooling is 38 °C, thus meeting the needs of the fuel cell air supply subsystem.

(4) Screw compressors can only achieve the same discharge volume flow as scroll compressors at a rapid speed. At the same volume flow, the rotational speed, discharge temperature, and noise of scroll compressors are lower than screw compressors. Due to the increase in the diameter of the orbiting and fixed scroll discs of the oil-free double-wrap scroll compressor, the structure of the whole machine will increase accordingly, which will increase the power of the compressor drive motor. Double-wrap scroll compressors are suitable for applications with large displacement and low pressure ratio.

Author Contributions: Investigation, J.S.; data Curation, J.S.; writing—original draft preparation, J.S.; writing—review and editing, B.P. and B.Z. All authors have read and agreed to the published version of the manuscript.

Data Availability Statement: Not applicable.

Conflicts of Interest: The authors declare no conflict of interest.

Abbreviations

SC1	Prototype 1—scroll compressor
SC2	Prototype 2—scroll compressor
SC3	Prototype 3—screw compressor
PEMFC	Proton Exchange Membrane Fuel Cells
HFC	Hydrogen Fuel Cell
CFD	Computational Fluid Dynamics
UDF	User Defined Function

References

1. Liu, M.Y.; Xiao, X.D.; Li, Q.; Luo, L.Y.; Ding, M.H.; Zhang, B.; Li, Y.X.; Zou, J.L.; Jiang, B.J. Recent progress of electrocatalysts for oxygen reduction in fuel cells. *J. Colloid Interface Sci.* **2021**, *607*, 791–815. [CrossRef] [PubMed]
2. Xie, X.S.; Yang, W.J.; Shi, W.; Zhang, S.S.; Wang, Z.S.; Zhou, J.H. Life cycle assessment of technologies for hydrogen production—A review. *Chem. Ind. Eng. Prog.* **2018**, *37*, 2147–2158.
3. Wiartalla, A.; Pischinger, S.; Bornscheuer, W.; Fieweger, K.; Ogrzewalla, J. Compressor expander units for fuel cell systems. *SAE Trans.* **2000**, *109*, 484–488.
4. Shao, Z.G.; Yi, B.L. Developing Trend and Present Status of Hydrogen Energy and Fuel Cell Development. *Bull. Chin. Acad. Sci.* **2019**, *34*, 469–477.
5. Ahmed, K.; Nikola, S.; Ian, S. *Screw Compressors*; Springer: Berlin/Heidelberg, Germany, 2007.
6. Wang, Z.L.; Wang, H.; Wang, Z.M.; Li, Q.; Feng, Q.K. Theoretical study on heat transfer characteristics of single screw refrigeration compressor with Multicolumn envelope meshing pair. *Appl. Therm. Eng.* **2019**, *166*, 114635. [CrossRef]
7. Gu, Z.L.; Yu, Y.Z.; Jiang, D.M. Improved Characteristics of Scroll Machines with Multiple Spiral. *J. Xi'an Jiaotong Univ.* **1998**, *32*, 90–93.
8. Wang, J.; Li, X.Q. Construction Theories of Meshing Profile for Multi-Wraps Scroll Machinery. *J. Mech. Eng.* **2008**, *44*, 74–79. [CrossRef]
9. Wang, J.; Ju, H.; Zhao, M.; Qu, Y. Influence of Wrap Number on Performance of Multi-Wrap Scroll Compressor. *J. China Univ. Pet. (Ed. Nat.Sci.)* **2009**, *33*, 118–122.
10. Peng, B.; Zhang, Y.B.; Zhang, P.C.; Zhang, Y.B.; Yin, B. Effects of Various Profile Parameters on the Performance of a Double-Scroll Compressor. *Chin. Hydraul. Pneum.* **2020**, *10*, 145–150.
11. Cardone, M.; Gargiulo, B. Numerical Simulation and Experimental Validation of an Oil Free Scroll Compressor. *Energies* **2020**, *13*, 5863. [CrossRef]
12. Chang, J.C.; Chang, C.W.; Hung, T.C.; Lin, J.R.; Huang, K.C. Experimental study and CFD approach for scroll type expander used in low-temperature organic Rankine cycle. *Appl. Therm. Eng.* **2014**, *73*, 1444–1452. [CrossRef]
13. Wang, J.; Song, Y.X.; Li, Q.; Zhang, D.H. Novel structured dynamic mesh generation for CFD analysis of scroll compressors. *Proc. Inst. Mech. Eng. Part A J. Power Energy* **2015**, *229*, 1007–1018. [CrossRef]

14. Ooi, K.T.; Zhu, J. Convective heat transfer in a scroll compressor chamber: A 2-D simulation. *Int. J. Therm. Sci.* **2004**, *43*, 677–688. [CrossRef]

15. Wang, J.; Song, Y.X.; Jiang, Y.; Li, Q.; Zhang, D.H. Numerical simulations of internal flow fields for scroll compressors based on structured dynamic meshes. *J. Eng. Thermophys.* **2016**, *37*, 309–313.

16. Wang, J.; Song, Y.X.; Zha, H.B.; Li, Q. 3D Numerical Simulation and Study of Discharge Process for Scroll Compressors. *J. Eng. Thermophys.* **2016**, *37*, 766–769.

17. Sun, S.H.; Wu, K.; Guo, P.C.; Yan, J.C. Analysis of the three-dimensional transient flow in a scroll refrigeration compressor. *Appl. Therm. Eng.* **2017**, *127*, 1086–1094. [CrossRef]

18. Zhao, R.C.; Li, W.H.; Zhuge, W.L. Unsteady characteristic and flow mechanism of a scroll compressor with novel discharge port for electric vehicle air conditioning. *Int. J. Refrig.* **2020**, *118*, 403–414. [CrossRef]

19. Fadiga, E.; Casari, N.; Suman, A.; Pinelli, M. Structured Mesh Generation and Numerical Analysis of a Scroll Expander in an Open-Source Environment. *Energies* **2020**, *13*, 666. [CrossRef]

20. Cavazzini, G.; Giacomel, F.; Ardizzon, G.; Casari, N.; Fadiga, E.; Pinelli, M.; Suman, A.; Montomoli, F. CFD-based optimization of scroll compressor design and uncertainty quantification of the performance under geometrical variations. *Energy* **2020**, *209*, 118382. [CrossRef]

21. Rak, J.; Pietrowicz, S. Internal flow field and heat transfer investigation inside the working chamber of a scroll compressor. *Energy* **2020**, *202*, 117700. [CrossRef]

22. Cavazzini, G.; Giacomel, F.; Benato, A.; Nascimben, F.; Ardizzon, G. Analysis of the Inner Fluid-Dynamics of Scroll Compressors and Comparison between CFD Numerical and Modelling Approaches. *Energies* **2021**, *14*, 1158. [CrossRef]

23. Zheng, S.Y.; Wei, M.S.; Song, P.P.; Hu, C.X.; Tian, R. Thermodynamics and flow unsteadiness analysis of trans-critical CO_2 in a scroll compressor for mobile heat pump air-conditioning system. *Appl. Therm. Eng.* **2020**, *175*, 115368. [CrossRef]

24. Zheng, S.Y.; Wei, M.S.; Chenxing, H.U.; Song, P.P.; Tian, R. Flow characteristics of tangential leakage in a scroll compressor for automobile heat pump with CO_2. *Sci. China Technol. Sci.* **2021**, *64*, 971–983. [CrossRef]

25. Wang, J.; Cui, S.J.; Feng, H.Z.; Li, H.X.; Sha, R.D. Construction and Simulation of An Asymmetric Twin-Wrap Profile for Scroll Compressor. *J. Eng. Thermophys.* **2021**, *42*, 386–392.

26. Versteeg, H.K.; Malalasekera, W. *An Introduction to Computational Fluid Dynamics: The Finite Volume Method*; Pearson Education: London, UK, 2007.

27. Park, I.; Choi, S.; Lee, B.; Yoo, B. Scroll Compressor with an Arcuate and a Logarithmic Spiral Sections. U.S. Patent 9,605,675B2, 2 March 2017.